OUTFLOWS FROM YSO'S AND THE ANGULAR MOMENTUM OF NEW-BORN STARS

Kohji Tomisaka

National Astronomical Observatory, Mitaka, Tokyo 181-8588, Japan; e-mail: tomisaka@th.nao.ac.jp

ABSTRACT

Dynamical collapses of magnetized molecular cloud cores are studied with magnetohydrodynamical simulations from the run-away collapse phase to the accretion phase. Owing to the large dynamic range covered by the nested-grid method, the structure of the cloud in the range from 10 AU to 0.1 pc is explored. In the run-away collapse phase, a disk threaded by magnetic field lines is contracting due to its self-gravity and its evolution is well expressed by a self-similar solution. The central density increases greatly in a finite time scale and reaches a density at which an opaque core is formed at the center. After that, matter accrets to the newly formed core (accretion phase). In this stage, a rotationally supported disk is formed in a cloud core without magnetic fields. In contrast, the disk continues to contract in the magnetized cloud core, since the magnetic fields transfer angular momentum from the disk. Its rotation motion winds up the threading magnetic field lines. Eventually, strong toroidal magnetic fields are formed and begin to drive the outflow, even if there is no toroidal field component initially. Bipolar molecular outflows observed in protostar candidates are naturally explained by this model.

If the angular momentum of the molecular cloud core were conserved during the star formation process, a new-born star would rotate much faster than its fission speed. This constitutes the angular momentum problem of new-born stars. The angular momentum transfer in the contraction of a rotating magnetized cloud is also studied with the MHD simulations. It is shown that in the run-away collapse phase, the specific angular momentum j of the disk decreases to $\simeq 1/3$ of the initial cloud. However, this is not insufficient to solve the angular momentum problem. After the central density of the disk exceeds $\sim 10^{10}\mathrm{cm}^{-3}$, the infall on to the central object develops. In this accretion stage, the rotation motion and thus the toroidal magnetic field drive the outflow. The angular momentum of the central object is transferred efficiently by the outflow as well as the effect of the magnetic stress. In 7000 yr from the core formation, the specific angular momentum of the central $0.17 M_\odot$ decreases a factor of 10^{-4} from the initial value (i.e. from $10^{20}\mathrm{cm}^2 \mathrm{s}^{-1}$ to $10^{16}\mathrm{cm}^2 \mathrm{s}^{-1}$).

Key words: ISM: clouds – ISM: jets and outflows – ISM: magnetic fields – stars: formation – stars: rotation

1. INTRODUCTION

The problem of star formation has been the object of serious study for many years. In the star formation process, almost all the angular momentum should be removed from the molecular cloud in the course of forming stars. For example, using rotation periods and the radius of classical T Tauri stars (CTTS) [$P = 3 - 10$ days and $R_* \simeq 2R_\odot$ (Bouvier et al. 1993)], the specific angular momentum of such stars is approximately equal to $j \simeq 4\pi R_*^2/(5P) \sim 5.6 \times 10^{16}\mathrm{cm}^2 \mathrm{s}^{-1}(R_*/2R_\odot)^2(P/10\mathrm{day})^{-1}$, where we assumed the star rotates uniformly. On the other hand, if the velocity gradient of $0.3\mathrm{km}\ \mathrm{s}^{-1}\ \mathrm{pc}^{-1} - 4\mathrm{km}\ \mathrm{s}^{-1}\ \mathrm{pc}^{-1}$ (Goodman et al. 1993) observed in $\mathrm{NH_3}$ cores (density $\gtrsim 10^4\mathrm{cm}^{-3}$; size ~ 0.1 pc) comes from the rotation, j reaches $\sim 5 \times 10^{21}\mathrm{cm}^2\ \mathrm{s}^{-1}(R/0.1\mathrm{pc})^2(\Omega/4\mathrm{km}\ \mathrm{s}^{-1}\ \mathrm{pc}^{-1})$. Therefore, the specific angular momentum should decrease a factor of 10^{-5} when a star is formed from a molecular cloud core. Assuming j is conserved through the collapse, the gravity is balanced with the centrifugal force at the centrifugal radius as $R_c = j^2/(GM) \sim 0.06\mathrm{pc}(j/5 \times 10^{21}\mathrm{cm}^2\ \mathrm{s}^{-1})^2(M/1M_\odot)^{-1}$. This leads to the conclusion that if the angular momentum is not efficiently reduced or transferred, the cloud could not shrink to become a stellar object ($R_c \gg R_*$). This is called the angular momentum problem for new-born stars.

To reduce the spin angular momentum of newly formed stars, two mechanisms are proposed. One is to transfer the cloud spin angular momentum to the orbital angular momentum of binary or multiple protostars if they are made by fission. The other possibility is magnetic braking, in which angular momentum is transferred to the ambient medium by the magnetic stress (Spitzer 1978). The latter works even for the case of a single star. In the case of the parallel rotator, in which the directions of magnetic fields and angular momentum coincide with each other, the time scale of deceleration of the angular rotation speed (Ω) is given by

$$t_B \equiv -\frac{\Omega}{d\Omega/dt} \simeq \frac{\sigma}{2\rho_a V_A} = \frac{2\pi G\sigma}{B_0}(4\pi G\rho_a)^{-1/2}, \qquad (1)$$

where σ, ρ_a, V_A, and G denote, respectively, the column density of the molecular core, the ambient density, the

Alfvén speed of the ambient medium, and the gravitational constant (Ebert, von Hoerner, & Temesvary 1960, Mouschovias, & Paleologou 1980). As long as the molecular core evolves in a quasistatic manner, the decrease in the angular momentum L is well fitted by the above time scale as $L = L(t = 0) \exp(-t/t_B)$ (Tomisaka, Ikeuchi, & Nakamura 1990). Since the first factor $2\pi G\sigma/B_0$ is approximately equal to or larger than unity for a gravitationally contracting cloud (Tomisaka 1995), t_B is longer than the free-fall time of the ambient low-density medium. This raises the question of whether or not the angular momentum is efficiently transferred while the contraction proceeds.

Recently, bipolar outflows have been found in a wide variety of objects which indicate star formation (for a review, see Bachiller 1996). Based on the magnetic acceleration model of outflow (Blandford, & Payne 1982; see also Königl 1989 and Wardle, & Königl 1993), magnetic fields extract the angular momentum from the disk and transfer it to the outflow gas. Therefore, the outflow gas is able to carry the excess angular momentum directly.

From MHD simulations of the gravitational contraction of a magnetized, rotating isothermal molecular cloud, it is shown that the outflow begins after the central density exceeds 10^{10}cm^{-3} and an adiabatic core forms in the center (Tomisaka 1998, hereafter Paper I). The outflow is never driven in the run-away collapse phase, since rotation motion and thus toroidal magnetic fields are unimportant in this phase. Therefore, in this paper, we study the evolution of the cloud from the runaway collapse phase to the accretion phase, continuously. In particular, we try to determine when the redistribution of angular momentum occurs and whether the outflow plays an important role in extracting the angular momentum from the contracting gas. The model and the numerical method are described in §2. In § 3, numerical results on the dynamical contraction of the magnetized rotating molecular cloud cores are shown. The condition to initiate the outflow is also presented. In § 4, the evolution of the specific angular momentum distribution is shown. In addition, a comparison is made between the effects of the magnetic torque and outflow to reduce the angular momentum. We discuss the ideal MHD condition and the evolution of late stage also in §4.

2. Model and Numerical Method

We began our simulation from an infinitely long, cylindrical, rotating, isothermal cloud in hydrostatic balance. In terms of the gravitational potential, ψ_0, the magnetic flux density, $\mathbf{B}_0 = B_z \mathbf{e}_z$, the angular rotation speed, Ω_0, and the density ρ_0, the hydrostatic configuration is governed by the equations

$$r\Omega_0^2 - \frac{d\psi_0}{dr} - \frac{c_s^2}{\rho_0}\frac{d\rho_0}{dr} - \frac{1}{8\pi}\frac{dB_z^2}{dr} = 0, \tag{2}$$

$$\frac{1}{r}\frac{d}{dr}\left(r\frac{d\psi_0}{dr}\right) = 4\pi G\rho_0. \tag{3}$$

These equations have a solution for the radial distributions of density, rotational velocity, and magnetic flux density as follows (Stodółkiewicz 1963):

$$\rho_0(r) = \rho_{c\,0}\left[1 + r^2/(8h^2)\right]^{-2}, \tag{4}$$

$$v_\phi(r) \equiv r\Omega_0(r) = r\Omega_c\left[1 + r^2/(8h^2)\right]^{-1/2}, \tag{5}$$

$$B_z(r) = B_c\left[1 + r^2/(8h^2)\right]^{-1}, \tag{6}$$

where h represents the central density scale-height as $4\pi G\rho_{c\,0}h^2 = c_s^2 + B_c^2/(8\pi\rho_{c\,0}) + 2\Omega_c^2 h^2$ for $\Omega_c < (2\pi G\rho_{c\,0})^{1/2}$. Here, quantities with a subscript c denote those for the cloud center ($r = 0$). This hydrostatic solution contains two nondimensional parameters: $\omega \equiv \Omega_c/(4\pi G\rho_{c\,0})^{1/2}$ and $\alpha \equiv B_c^2/(4\pi\rho_{c\,0}c_s^2)$.

We assume that the gas obeys the ideal MHD equations. The gas is assumed isothermal for low densities. However, after the density exceeds $\sim 10^{10}$cm^{-3}, the interstellar gas is not efficiently cooled and behaves adiabatically (Larson 1969). To mimic this situation, a barotropic relation such as

$$p \begin{cases} = c_s^2\rho, \dots (\rho < \rho_{\text{crit}}) \\ = c_s^2\rho_{\text{crit}}(\rho/\rho_{\text{crit}})^\Gamma, \dots (\rho > \rho_{\text{crit}}) \end{cases} \tag{7}$$

was adopted without using the energy equation, where we take $\rho_{\text{crit}} = 10^{10}H_2$cm^{-3}. The polytropic exponent Γ was taken as $5/3$ and 2. (The specific heat ratio γ never exceeds $5/3$. However, we found that the flow outside the core and the mass-accretion rate are essentially the same irrespective of the values of the core's polytropic exponent, Γ. Therefore, we used the larger exponent to reduce the effort to perform numerical computations.) To initiate gravitational contraction, we added density perturbation with small amplitude. The periodic boundary condition was applied to the boundaries in the z-direction, and the separation between two boundaries was chosen to be identical with the wavelength of the gravitationally most unstable mode (Matsumoto, Hanawa, & Nakamura 1997). To ensure the fine spatial resolution necessary especially near the forming adiabatic core, the nested-grid method was applied to the MHD finite difference scheme (Tomisaka 1996a, 1996b, 1998). In the nested-grid method, 15 levels of grids are used from L0 (the coarsest) to L14 (the finest). A grid spacing of Ln was chosen as $1/2$ of that of L$n - 1$, and each level of grids was divided into 64×64 cells. The code was tested by comparing the result of gravitational collapse calculated by a code without the nested-grid method (for details, see Tomisaka 1996b).

3. RESULTS

Here, the results of the model with $\omega = 1/2$, $\alpha = 1$ and $\rho_{c\,0} = 100\rho_s$ (ρ_s represents the density at the surface of the cloud) are shown. This corresponds to $\Omega = 2.78n_{s\,2}^{1/2}$ km s^{-1} pc^{-1} and $B_c = 13.3n_{s\,2}^{1/2}c_{s\,190}\,\mu$G. Here,
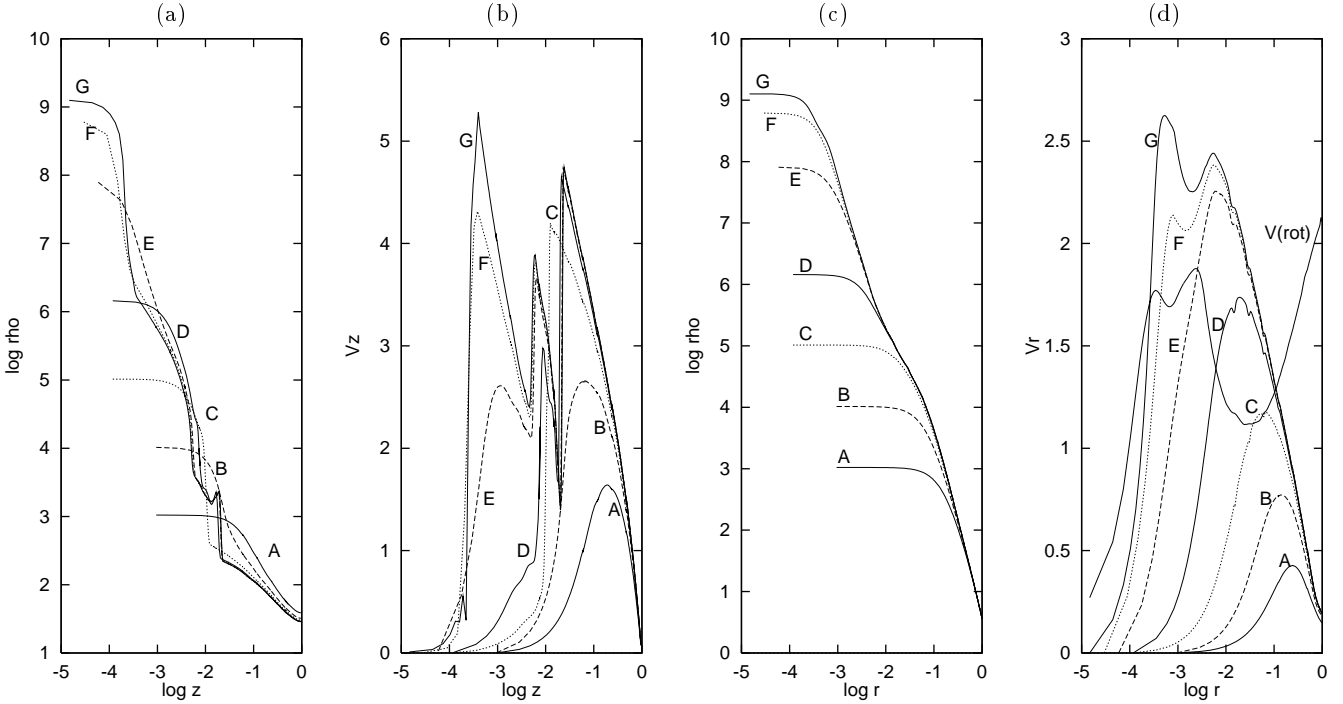
Figure 1. Distributions of the density and infall speed along the z-axis are plotted in (a) $\log \rho(z, r = 0)$ and (b) $|v_z(z, r = 0)|$ respectively. Those along the equatorial plane are also shown in (c) $\log \rho(z = 0, r)$ and (d) $|v_r(z = 0, r)|$. Snapshots are made at $t = 0.5233\tau_{\mathrm{ff}} \simeq 0.916 n_{s\,2}^{-1/2}$ Myr ($\rho_c \sim 10^3 \rho_s \simeq 10^5 n_{s\,2}$ $H_2 \mathrm{cm}^{-3}$: A), $t = 0.5725\tau_{\mathrm{ff}} \simeq 1.002 n_{s\,2}^{-1/2}$ Myr ($\rho_c \sim 10^4 \rho_s \simeq 10^6 n_{s\,2}$ $H_2 \mathrm{cm}^{-3}$: B), $t = 0.5908\tau_{\mathrm{ff}} \simeq 1.034 n_{s\,2}^{-1/2}$ Myr ($\rho_c \sim 10^5 \rho_s \simeq 10^7 n_{s\,2}$ $H_2 \mathrm{cm}^{-3}$: C), $t = 0.5977\tau_{\mathrm{ff}} \simeq 1.046 n_{s\,2}^{-1/2}$ Myr ($\rho_c \sim 10^6 \rho_s \simeq 10^8 n_{s\,2}$ $H_2 \mathrm{cm}^{-3}$: D), $t = 0.5994\tau_{\mathrm{ff}} \simeq 1.049 n_{s\,2}^{-1/2}$ Myr ($\rho_c \sim 10^8 \rho_s \simeq 10^{10} n_{s\,2}$ $H_2 \mathrm{cm}^{-3}$: E), $t = 0.5996\tau_{\mathrm{ff}} \simeq 1.049 n_{s\,2}^{-1/2}$ Myr ($\rho_c \sim 10^{8.8} \rho_s \simeq 10^{10.8} n_{s\,2}$ $H_2 \mathrm{cm}^{-3}$: F), and $t = 0.5997\tau_{\mathrm{ff}} \simeq 1.049 n_{s\,2}^{-1/2}$ Myr ($\rho_c \sim 10^{9.1} \rho_s \simeq 10^{11.1} n_{s\,2}$ $H_2 \mathrm{cm}^{-3}$: G). Rotation velocity distribution along the equatorial plane is plotted for the epoch G in (d).

$n_{s\,2}$ and $c_{s\,190}$ represent respectively $\rho_s / 10^2 H_2\ \mathrm{cm}^{-3}$ and $c_s / 190 \mathrm{m\ s}^{-1}$. Hereafter we use distance and time normalized by $H \equiv c_s / (4\pi G \rho_s)^{1/2} = 0.36 c_{s\,190} n_{s\,2}^{-1/2}$ pc and $\tau_{\mathrm{ff}} \equiv 1 / (4\pi G \rho_s)^{1/2} = 1.75 n_{s\,2}^{-1/2}$ Myr, respectively.

3.1. Run-away Collapse Phase

The evolution is similar to that of magnetized cloud with no rotation (Tomisaka 1995, 1996a; Nakamura, Hanawa, & Nakano 1995). First, the cylindrical cloud breaks into prolate spheroidal fragments which is elongated along the cylinder axis (z-axis). As long as the amplitude of density perturbation is small $\delta\rho/\rho \lesssim 1$, the shape keeps essentially identical with the most unstable eigen-function of the gravitational instability. Next, gas begins to fall mainly along the magnetic field, and forms a disk perpendicular to the magnetic fields. The disk formed in a runaway collapse is far from static balance. However, the flow is controlled under the magnetic field and centrifugal force which lead to disk structure (pseudo-disk: Galli & Shu 1993). At $t = 0.5908\tau_{\mathrm{ff}} \simeq 1.034 n_{s\,2}^{-1/2}$ Myr, at that time the central density ρ_c reaches $\simeq 10^5 \rho_s = 10^7 n_{s\,2}$ $H_2\ \mathrm{cm}^{-3}$, a shock wave is formed parallel to the disk (see Line C of Figs.1a & 1b). It breaks into two waves at the epoch when

the central density reaches $\rho_c \sim 10^6 \rho_s = 10^8 n_{s\,2}$ $H_2\ \mathrm{cm}^{-3}$: an outer wave front propagates outwardly as a fast-mode MHD shock (seen near $z \sim 0.02H \simeq 1400 c_{s\,190} n_{s\,2}^{-1/2}$ AU) and an inner one does inwardly as a slow-mode MHD shock (seen near $z \sim 7 \times 10^{-3} H \simeq 500 c_{s\,190} n_{s\,2}^{-1/2}$ AU) reaching the equator. The rotation angular speed Ω and toroidal magnetic field component B_ϕ also jump crossing the wave fronts. Fast rotation and thus strong B_ϕ are observed in a restricted region between these two fronts. Since the disk contracts in the radial direction, it has a larger Ω than outside the disk. In this configuration, magnetic fields may transfer the angular momentum from the disk and redistribute it into the same magnetic flux tube (magnetic braking). However, from this numerical simulation it is shown that the angular momentum is confined into a region inside the fast-mode MHD shock fronts.

Although there exists a number of shock waves ($z \sim 0.02H \simeq 1400 c_{s\,190} n_{s\,2}^{-1/2}$ AU, $5 \times 10^{-3} H \simeq 360 c_{s\,190} n_{s\,2}^{-1/2}$ AU, and $2 \times 10^{-4} H \simeq 14 c_{s\,190} n_{s\,2}^{-1/2}$ AU) propagating in the z-direction, no such discontinuity is found in the r-direction (Figs.1c & 1d). However, a kind of modulation is seen around a power-law distribution as $\rho(z = 0, r) \propto r^{-2}$, which is related to the formation of multiple shock waves in the z-direction (this is found by Norman et al (1980) for
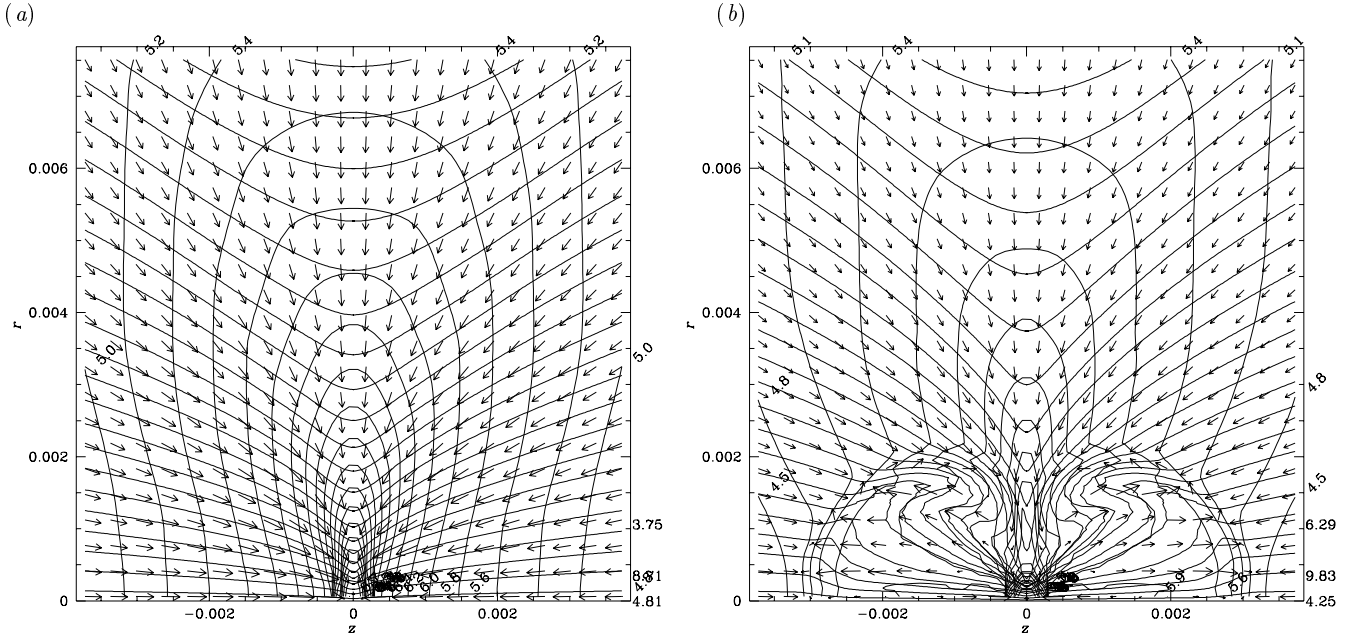
(a)

(b)

Figure 2. Left: isodensity lines, magnetic field lines, and velocity vectors are plotted for the state when the central density reaches $10^{8.8}\rho_s \simeq 10^{10.8}n_{s\,2}$ $H_2 cm^{-3}$ ($t = 0.5996\tau_{ff} \simeq 1.049n_{s\,2}^{-1/2}$ Myr). In contrast to the usual usage, the z-axis is placed horizontally and the r-axis is vertically. Right: the same as (a) but for the state when the central density reaches $10^{10}\rho_s \simeq 10^{12}n_{s\,2}$ $H_2 cm^{-3}$ ($t = 0.6002\tau_{ff} \simeq 1.050n_{s\,2}^{-1/2}$ Myr). Both are Level 8. Physical time passed between these two is equal to $1000n_{s\,2}^{-1/2}$ yr.

the case of rotating nonmagnetized isothermal cloud). The run-away collapse continues till $t \simeq 0.6\tau_{ff} \simeq 1.05n_{s\,2}^{-1/2}$ Myr and the central density would increase greatly if the isothermal equation of state continues to be valid. However, when the central density exceeds $\sim 10^{10} cm^{-3}$, the central part of the core becomes optically thick for the thermal radiation from dusts and its temperature begins to rise (for example, Masunaga, Miyama, & Inutsuka,1998).

3.2. ACCRETION PHASE

In the accretion phase, gas continues to accretes onto the newly formed opaque core. We mimic the situation by using a double polytrope shown in equation (7). We take $\rho_{\rm crit} = 10^8\rho_s = 10^{10}n_{s\,2} cm^{-3}$ and $\Gamma = 5/3$. By virtue of this assumption we can follow further evolution. Figure 2a shows the structure captured by L8 just after the isothermal equation of state is broken. A disk, which runs vertically, contracts radially and gas motion drags and squeezes the magnetic field lines to the center. The rotation speed v_ϕ at that time is not more than the radial infall speed v_r which is in the range of $(2-3) \times c_s$ (see Fig. 1d).

In the accretion phase, the inflow speed is accelerated at least to $(4-5) \times c_s$ and as a result magnetic field lines are strongly dragged and squeezed to the center (see Fig.1c of Tomisaka 1996b). Beside these, the rotation speed is accelerated as the infall proceeds. Just after the state shown in Figure 1 with the highest central concentration, v_ϕ reaches $\simeq 4c_s$ at the distance of $r \sim 3 \times 10^{-4}H \simeq 20c_{s\,190}n_{s\,2}^{-1}$ AU

inside of which a nearly spherical core is formed supported mainly by thermal pressure. The rotation velocity v_ϕ exceeds the radial velocity v_r in the accretion phase, while v_ϕ was smaller than v_r (see Fig. 1d) in the run-away collapse phase. From this epoch, outflow from the disk is observed.

Figure 2 shows the structures before (a) and after (b) the outflow begins. The physical time scale between Figures 2a and 2b is approximately equal to $\simeq 1000n_{s\,2}^{-1/2}$ yr. The directions of the magnetic fields in the disk is much affected by the radial inflow. They are pushed and squeezed to the center. It is shown that in the seeding region of the outflow the angle between a magnetic field line and the disk plane decreases from $60° - 70°$ (Fig.2a) to $10° - 30°$ (Fig.2b). In Figure 2b, it is indicated that the outflow, which reaches $z_s \sim \pm 0.003H \simeq \pm 200 AU(H/0.36 pc)$, is confined into two expanding bubbles whose centers are at $z_c \sim \pm 0.0015H \simeq \pm 100 AU(H/0.36 pc)$. In the bubble, the strength of toroidal component of magnetic fields B_ϕ is larger than that of the poloidal one $(B_z^2 + B_r^2)^{1/2}$. Especially at the outer boundary of the bubble $|B_\phi|$ is $(4-5)$ times stronger than $(B_z^2 + B_r^2)^{1/2}$ (see also the upper panel of Fig. 3). Further, the magnetic pressure is much larger than the thermal one. Outside of the bubble, inflow continues. The islands of strong toroidal magnetic fields which are formed just outside the disk push the poloidal fields and have an effect to strengthen the hourglass structure in the poloidal field (Ouyed & Pudritz 1997).

To see the seeding region of the outflow closely, we plot a close-up view captured by L10 in Figure 3. (Seeding re-
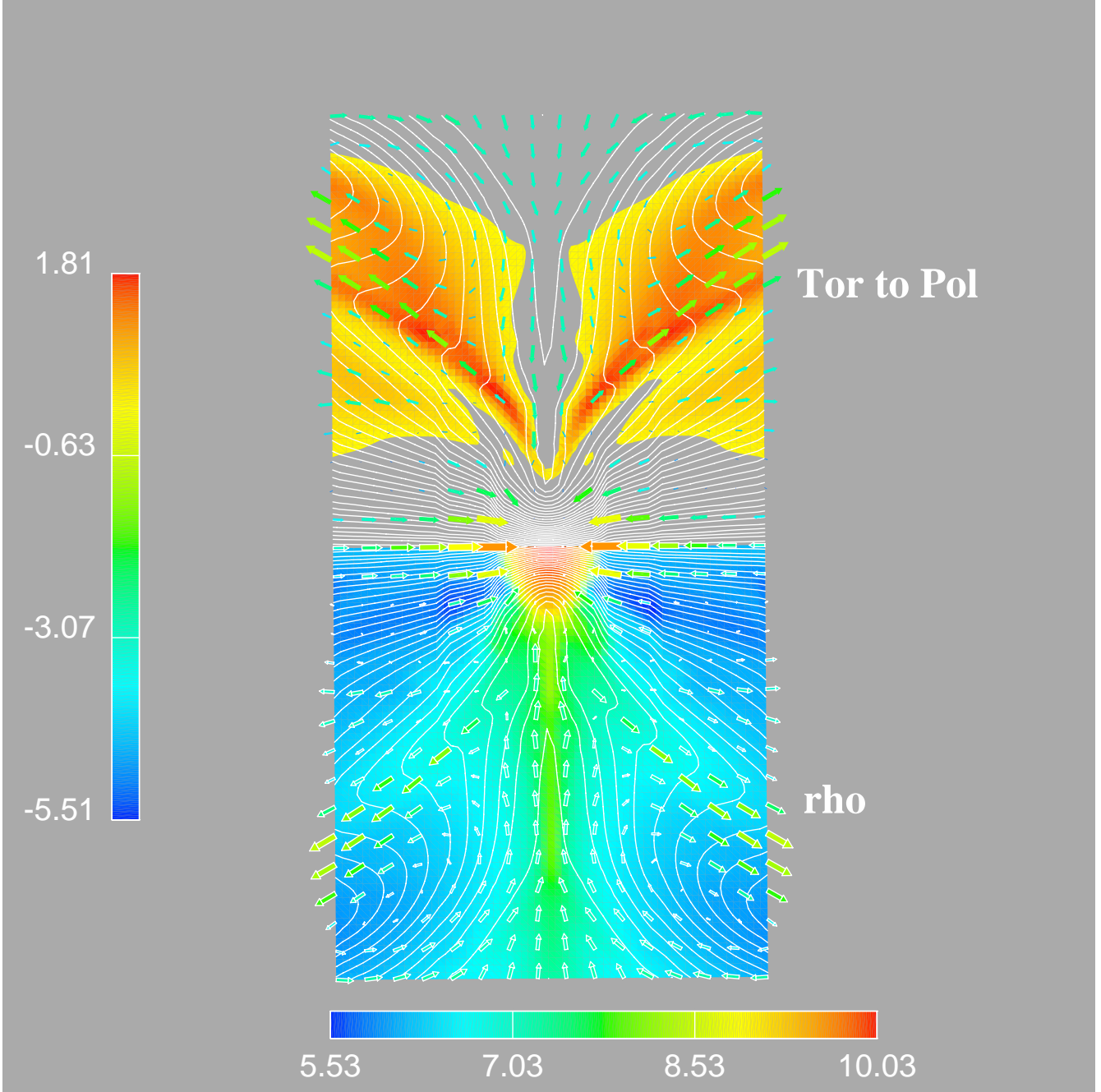
Figure 3. Close-up view of the seeding region of the outflow. False colors represent the ratio of the toroidal magnetic pressure $B_\phi^2/8\pi$ to the poloidal one $(B_z^2 + B_r^2)/8\pi$ in the upper panel and the density distribution ρ in the lower panel, respectively. Velocity vectors (v_z, v_r) and magnetic field lines (B_z, B_r) are also plotted. This figure shows Level 10 which has 4-times finer spatial resolutions than the previous one $(-10^{-3}H \le z \le 10^{-3}H$ and $0 \le r \le 2 \times 10^{-3}H)$.

gion, from which outflow is ejected, moves outwardly with time. In the disk, the ratio of the centrifugal force to the gravity is no more than $\simeq 0.45$. It indicates this is far from centrifugal balanced state.) This figure shows that the outflow is ejected from the disk near $r \simeq 5 \times 10^{-4}H \simeq 40\mathrm{AU}(H/0.36\mathrm{pc})$, which is 5 times larger than the scale length for the critical density $\rho_{\mathrm{cr}} = 10^{10}\mathrm{cm}^{-3}$. Figure 3 clearly shows that (1) magnetic field lines are almost par-

allel to the disk surface near the disk. (2) gas inflow in the disk is not disturbed by the outflow from the disk and continues to reach the central core which is supported by the thermal pressure. (3) outflow occurs along magnetic field lines whose inclination angle is in the range of $45°$ - $60°$. This corresponds to the region where $|B_\phi|$ is dominant over the poloidal component (upper panel).

Consider the main outflow ejected from $r \simeq 5 \times 10^{-4} H \simeq$ 40AU($H/0.36$pc) in Figure 3. Numerical simulations (Kudoh, Matsumoto, & Shibata 1998; Ouyed & Pudritz 1997) indicate that the ratio of Alfven speed to the rotation speed is controlling how the matter is accelerated. Since this ratio is small as $0.3 - 1$ in the seeding region $r \sim 5 \times 10^{-4} H$, it is natural that the toroidal magnetic field is strongly amplified just outside of the disk. In this case, the magnetic pressure gradient is considered to play an important role to accelerate the gas after the Alfven points located near $|z| \sim 10^{-4} H$. (In contrast, the matter is centrifugally driven when the ratio is large.) However, even in the present model, gas seems to escape from the disk with being driven centrifugally.

4. DISCUSSION

4.1. SPECIFIC ANGULAR MOMENTUM DISTRIBUTION

In Figure 4, the specific angular momentum j is plotted against the mass measured from the center. (Parameters are the same as the previous section except for Γ, the polytropic exponent for the adiabatic core. We take $\Gamma = 2$.) Since the density increases monotonically reaching the center, a mass shell with higher density is considered to be located nearer to the center than that with lower density. The total mass of the gas whose density is higher than ρ_1,

$$M(> \rho_1) = \int_{\rho > \rho_1} \rho(z, r) dV, \qquad (8)$$

and the correspondent total angular momentum,

$$L(> \rho_1) \equiv \int_{\rho > \rho_1} \rho(z, r) v_\phi r dV, \qquad (9)$$

are calculated at three epochs. Figure 4 is made by plotting $j(> \rho_1) \equiv L/M$ against $M(> \rho_1)$ for various ρ_1. This is similar to the specific angular momentum spectrum (e.g. Fig.5 of Norman, Wilson, & Barton 1980) in which $M(< j)$, the total mass whose specific angular momentum is smaller than j is plotted against j. However, the plot in Figure 4 has an advantage that the gas with smaller M is necessarily located nearer to the center.

Open circles represent the $j(< M)$ distribution in the early phase [$t = 0.5214(4\pi G\rho_s)^{-1/2} \sim 0.9 n_{s\,2}^{-1/2}$Myr], in which the central density increases a factor 10 from the initial state (i.e., ρ_c reaches $\simeq 10^5 n_{s\,2} H_2$ cm^{-3}). At this stage, the density distribution is almost spherical. Filled squares denote the distribution at the end of the run-away collapse phase ($t < 0.5980(4\pi G\rho_s)^{-1/2} \sim 1.05 n_{s\,2}^{-1/2}$Myr; the structure at the stage is shown in Fig. 2a). Since the motion crossing the magnetic fields is blocked, a disk running perpendicularly to the magnetic fields is formed. From Figure 4, it is shown that the angular momentum contained in the central $\sim 0.5 c_{s\,190}^3 n_{s\,2}^{-1/2} M_\odot$ is reduced to $\simeq 1/3$ before a core is formed.

This reduction is not owing to the angular momentum transfer by the magnetic fields but to the change of the shape of high-density region (from spherical to disk-like). This is confirmed by the fact that the specific angular momentum spectrum (not shown here) is not changed during the run-away collapse phase. The disk is mainly formed by the gas flow parallel to the magnetic fields (z-direction). Therefore, central part of the run-away collapsing disk is made by a gas with small angular momentum sitting initially near the z-axis. In other words, to the high-density region the mass is preferentially gathered rather than the angular momentum. The difference between open circles and filled squares in Figure 4 is owing to the segregation of low-angular momentum gas in the run-away collapse stage. However, the amount of the angular momentum segregation is too insufficient to explain the angular momentum problem.

The specific angular momentum, j, is approximately proportional to the accumulated mass, M. This relation coincides with the prediction for the thin disk by Basu(1998). This relation is explained from the solution of the contracting isothermal thin disk, i.e., the column density $\sigma \simeq c_s/Gr$ and the angular rotation speed $\Omega \propto r^{-1}$ (Matsumoto et al. 1997) lead to the specific angular momentum $j = \Omega r^2 \propto r \propto M \equiv \int \sigma r dr$.

After the central density of the disk exceeds $\rho_{\rm crit} \sim 10^{10} H_2$cm^{-3}, a new phase appears: the accretion phase. Thermal photons emitted from the dust which cooled the cloud become optically thick; as a result, an almost spherical adiabatic core is formed (in the adiabatic core, the thermal pressure becomes more important). Gas around the core begins to accrete on the core.

As shown in the previous section, after $\sim 10^3$ yr has passed, the outflow begins (Figs. 2b & 3). The size of the seeding region (origin of the outflow) is $r \sim 5 \times 10^{-4} H \sim 35 c_{s\,190} n_{s\,2}^{-1/2}$AU. The seeding region expands radially outward. This outflow is driven by the gradient of the magnetic pressure of the toroidal magnetic fields, $-\nabla B_\phi^2/8\pi$, which are made by the rotation motion (Paper I;Kudoh, Matsumoto, & Shibata 1998). The magnetic fields exert torque on the outflowing gas to increase its angular momentum. On the other hand, they exert torque on the disk to decrease the angular momentum (Blandford, & Payne 1982). In $\tau = 0.004(4\pi G\rho_s)^{-1/2} \sim 7000 n_{s\,2}^{-1/2}$yr (filled triangles; τ is the time elapsed from the core formation epoch), the outflow expands and reaches $z \sim 0.025 c_s (4\pi G\rho_s)^{-1/2} \sim 1800 c_{s\,190} n_{s\,2}^{-1/2}$AU. The angular momentum distribution at that time is shown by the solid line in Figure 4. It is shown that the specific angular momentum contained in the central $\sim 0.17 c_{s\,190}^3 n_{s\,2}^{-1/2} M_\odot$ ($\rho > 10^{10} n_{s\,2} H_2$ cm^{-3}) has been reduced to a factor $\lesssim 10^{-4}$ of the initial value.

4.2. ANGULAR MOMENTUM FLUX AND MAGNETIC TORQUES

Consider the total angular momentum, $L(< M)$, contained in the mass M. The increase and decrease of the
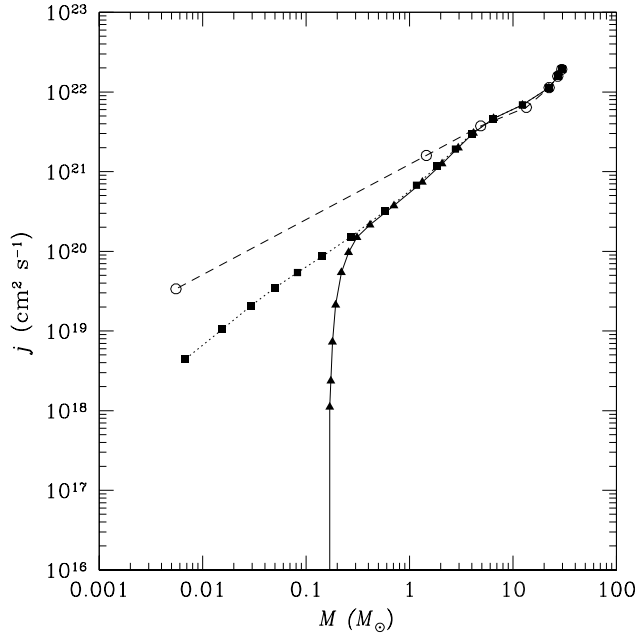
Figure 4. Specific angular momentum j is plotted against the accumulated mass from the center M. Open circles, filled squares, and triangles denote, respectively, the beginning and the end of the run-away collapse phase and the accretion phase.
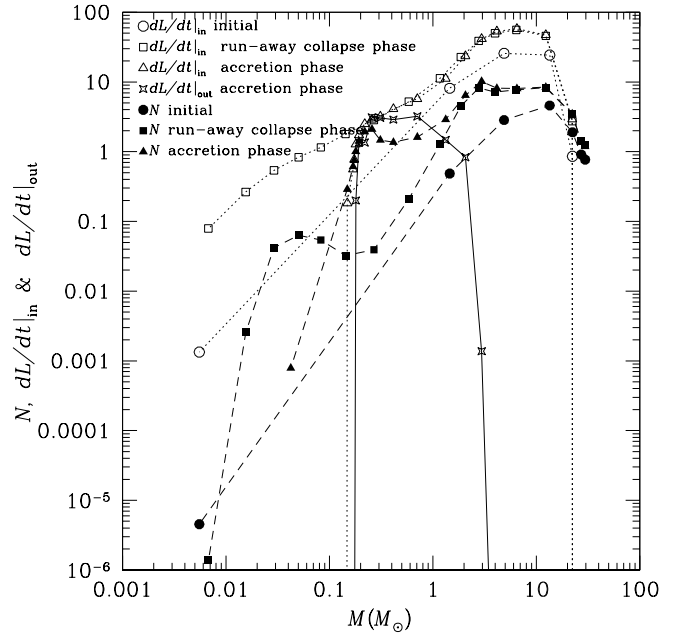

Figure 5. The torque exerted on the cloud core by the magnetic fields, N, the angular momentum inflow rate convected by the inflow in the disk, $dL/dt|_{in}$, and its outflow rate transferred by the outflow, $dL/dr|_{out}$. Filled and open symbols denote respectively the distribution of N and that of $dL/dt|_{in}$. The circles, and squares denote, respectively, the beginning and the end of the run-away collapse phase. Open stars represent the angular momentum outflow rate $dL/dt|_{out}$ in the accretion phase.

angular momentum are caused by (1) the inflow (accretion flow) mainly in the disk $dL/dt|_{in}$, (2) the torque exerted on the gas disk from the magnetic fields N, and (3) the outflow from the disk $dL/dt|_{out}$: $dL/dt = dL/dt|_{in} + dL/dt|_{out} + N$. It is to be noted that only the first term is positive. To see which term is important to reduce the angular momentum, we plot these three quantities for the three epochs in Figure 5. To calculate $dL/dt|_{in}$ and $dL/dt|_{out}$, we consider a cylinder which covers the isodensity surface. The $dL/dt|_{out}$ is measured by the angular momentum flux convected outwardly through the upper and lower surfaces of the cylinder, and $dL/dt|_{in}$ is the flux running radially inward through the side surface.

Before the core formation (circles and squares), the angular momentum inflow ($dL/dt|_{in}$) is larger than the magnetic torque (N) which reduces the angular momentum. (This does not mean that the specific angular momentum increases. Note that $dM/dt|_{in}$ is also positive.) In contrast, in the accretion phase after outflow blows, the magnetic torque (filled triangles) is comparable with $dL/dt|_{in}$ (open triangles) near $M \gtrsim 0.17c_{s\,190}^3 n_{s\,2}^{-1/2} M_\odot$ ($\tau = 7000n_{s\,2}^{-1/2}$yr). Further, from the figure, it is shown that the angular momentum transport by outflow $dL/dt|_{out}$ (open stars) is more efficient than that of the magnetic torque. By these two effects, the angular momentum transferred by the inflow inside the disk is totally removed for central $\sim 0.17c_{s\,190}^3 n_{s\,2}^{-1/2} M_\odot$. As a result, $j(< 0.17c_{s\,190}^3 n_{s\,2}^{-1/2} M_\odot)$ is reduced a factor of 10^{-4} from the initial value.

4.3. FURTHER EVOLUTION

The size of the outflow reaches $z \sim 0.025c_s/(4\pi G\rho_s)^{1/2} \sim 1800c_{s\,190}n_{s\,2}^{-1/2}$AU in $\tau \sim 7000n_{s\,2}^{-1/2}$yr. However, CO observations show that the molecular outflows have typical spatial size of 8000 AU $-$ 4 pc (Fukui et al. 1993). This simulation is limited in time and should be extended further. However, calculation becomes harder after the core mass exceeds $\sim 0.1c_{s\,190}^3 n_{s\,2}^{-1/2} M_\odot$ due to high density at the cloud center. Let us consider whether the magnetic angular momentum transport is effective still in the later stage $\tau > 7000n_{s\,2}^{-1/2}$yr.

As shown in Figure 1, j is approximately proportional to M at the epoch of the core formation. Writing down the relation as $j = p \times GM/c_s$, the coefficient p is approximately equal to 0.1 for the model shown in Figure 1. If j is conserved, the centrifugal radius (R_c), at which the gravity is balanced with centrifugal force, is given by $R_c = j^2/GM = p^2 GM/c_s^2 \sim 250(p/0.1)^2(M/1M_\odot)c_{s\,190}^{-2}$AU [a similar relation is pointed out by Basu (1998)]. This indicates that the centrifugal radius expands with time. On the other hand, a self-similar solution for the rotating isothermal thin disk has been found by Saigo & Hanawa (1998). Their solution in the accretion phase also shows that the radius where v_ϕ takes the maximum increases

with time as $\propto c_s \tau$. Since the outflow is ejected from a radius where v_ϕ is important (Paper I), these two indicate that the seeding region of the outflow moves outwardly. Using the solution by Saigo & Hanawa (1998; for an example, see their Figure 7), the surface density (Σ) and thus the density (ρ) decrease as collapse proceeds and the seeding region moves outwards. This shows that the density near the seeding region decreases as the collapse proceeds.

This leads to the conclusion that the coupling between gas and magnetic fields (Nakano 1990) becomes stronger as long as we consider the seeding region, indicating that the mechanism of angular momentum transfer works also in the later stage of the evolution.

REFERENCES

Bachiller, R. 1996, ARA&A, 34, 111.

Basu, S. 1998, ApJ, 509, 229.

Blandford, R.D., & Payne, D.G. 1982, MNRAS, 199, 883.

Bouvier, J., Cabrit, C., Fernández, M., Martín, E.L., & Matthews, J. 1993, A&A, 272, 176.

Ebert, R., von Hoerner, S., & Temesvary, S. 1960, Die Entstehung von Sternen durch Kondensation diffuser Materie, (Springer-Verlag, Berlin) p.315.

Fukui, Y., Iwata, T., Mizuno, A., Bally, J. & Lane, A.P. 1993, in Protostars and Planets III, eds. E.H. Levy, & J.J. Lunine (Tucson, University Arizona Press) p.603.

Goodman, A.A., Benson, P.J., Fuller, G.A., & Myers, P.C. 1993, ApJ, 406, 528.

Königl, A. 1989, ApJ, 342, 208.

Kudoh, T., Matsumoto, R., & Shibata, K. 1998, ApJ, 508, 186.

Larson, R.B. 1969, MNRAS, 145, 271.

Matsumoto, T., Hanawa, T., & Nakamura, F. 1997, ApJ, 478, 569.

Mouschovias, T.Ch., &Paleologou, E.V. 1980, ApJ, 237, 877.

Nakamura, F., Hanawa, T., & Nakano, T. 1995, ApJ, 444, 770

Nakano, T. 1990, MNRAS, 242, 535.

Norman, M.L., Wilson, J.R., & Barton, R.T. 1980, ApJ, 239, 968.

Saigo, K., & Hanawa, T. 1998, ApJ, 493, 342.

Spitzer, L.Jr. 1978, Physical Processes in the Interstellar Medium (Wiley, New York) §13.3.

Stodółkiewicz, J.S. 1963, Acta Astron., 13, 30.

Tomisaka, K. 1995, ApJ, 438, 226.

Tomisaka, K. 1996a, PASJ, 48, L97.

Tomisaka, K. 1996b, PASJ, 48, 701.

Tomisaka, K. 1998, ApJ, 502, L163 (Paper I).

Tomisaka, K., Ikeuchi, S., & Nakamura, T. 1990, ApJ, 362, 202.

Wardle, M., & Königl, A. 1993, ApJ, 410, 218.